




PROPERTIES OF SHORT-PERIOD INTERNAL WAVES IN THE KARA GATES STRAIT REVEALED FROM SPACEBORNE SAR DATA

I. O. Kopyshov^{1,2} , I. E. Kozlov¹ , A. I. Shiryborova^{3,5} , S. A. Myslenkov^{3,4,5} 

¹Marine Hydrophysical Institute of RAS, Sevastopol, Russia;

²Moscow Institute of Physics and Technology, Dolgoprudny, Russia;

³Lomonosov Moscow State University, Moscow, Russia;

⁴Hydrometcenter of Russia, Moscow, Russia;

⁵Shirshov Institute of Oceanology RAS, Moscow, Russia

* **Correspondence to:** I. Kopyshov, kopyshov.io@phystech.edu

Abstract: This paper presents the results of identification of surface manifestations (SM) of short-period internal waves (SIW) in Sentinel-1 A/B synthetic aperture radar (SAR) images of the Kara Gates Strait in August–September 2021. 44 SM of SIW trains were detected in 47 SAR images. Statistics of occurrence, propagation direction and spatial characteristics of SIWs in the study area are given. During two months, satellite observations cover almost all phases of spring-neap tidal cycle. The use of a detailed topography of the study area made it possible to identify certain regions with a more frequent presence of the SIW leading crests with a particular focus made on the shallow (< 100 m) part of the strait. Each identified region is then described in terms of water depth, dimensionless slope, amplitudes of tidal current velocity and properties of SIWs. The obtained results were then compared with the results of previous studies.

Keywords: short-period internal waves, SAR imaging of sea surface, barotropic tide, spring-neap cycle, Kara Gates Strait, Arctic Ocean.

Citation: Kopyshov I., Kozlov I., Shiryborova A., Myslenkov S. (2023), Properties of Short-Period Internal Waves in the Kara Gates Strait Revealed from Spaceborne SAR Data, *Russian Journal of Earth Sciences*, Vol. 23, ES0210, <https://doi.org/10.2205/2023ES02SI10>

1. Introduction

The problem of studying internal waves (IWs) in the Arctic region has been raised many times and is still relevant today, because it has an important practical application. The formation and further collapse of internal waves can lead to intensive mixing of water masses [D'Asaro, 2022; Fer et al., 2020; Phillips, 1980; Sabinin et al., 2004], vertical transport of heat and nutrients [Boegman and Stastna, 2019; Edge et al., 2021; Garwood et al., 2020; Moum et al., 2003, 2007; Pineda, 1991]. In addition, IWs in the Arctic region can directly affect the characteristics of sea ice [Carr et al., 2019; Czipott et al., 1991] and the formation of polynyas [Morozov and Pisarev, 2004].

A peculiar feature of IWs in the Arctic Ocean is their formation and propagation near the critical latitude [Kagan et al., 2018; Konyaev, 2000; Morozov and Paka, 2010; Morozov and Pisarev, 2002]. When approaching it, the internal tide (IT) at the main tidal frequency M_2 becomes unstable and cannot freely propagate far from the generation area. The final stage of the evolution of the IT is its destruction and generation of packets of short-period internal waves (SIWs). Due to the stability of wave packets as a separate structure, they can spread over long distances. This was confirmed by the analysis of satellite synthetic aperture radar (SAR) data [Kozlov et al., 2015a,b], on which surface manifestations (SM) of SIWs are visible in the form of alternating light and dark bands associated with the amplification and attenuation of the radar backscattering in surface current convergence and divergence zones [Kudryavtsev et al., 2014].

RESEARCH ARTICLE

Received: 20 October 2023

Accepted: 27 November 2023

Published: 15 December 2023



Copyright: © 2023. The Authors. This article is an open access article distributed under the terms and conditions of the Creative Commons Attribution (CC BY) license (<https://creativecommons.org/licenses/by/4.0/>).

The transformation of IT into SIW packets is associated with the instability of the former at high depth gradients. In simple linear two-dimensional case, the impingement of the IT on the underwater inhomogeneity generates a series of packets of SIWs running in the opposite direction [Jackson *et al.*, 2012; Li *et al.*, 2019; Morozov *et al.*, 2002]. In the real case, underwater inhomogeneities can have a very complex structure so that the direction of SIW propagation might change underway. Narrow ocean areas with fairly intense tidal dynamics are exactly such regions. One such example is the Kara Gates Strait (KGS) characterized by a complex bottom relief [Li *et al.*, 2019; Morozov and Frey, 2023; Morozov *et al.*, 2017] and a variety of directions for the distribution of SIW packages [Kozlov *et al.*, 2015a; Morozov *et al.*, 2017].

Considering the process of SIW generation, it is important to remind that the current flow regime is characterized by a dimensionless Froude number $Fr = u/c$, where u is the total vector of the flow velocity, and c is the phase velocity of long linear internal waves determined by background stratification. The formation of SIW packets occurs during the transition of Fr from subcritical ($Fr < 1$) to the supercritical flow mode ($Fr > 1$) [Maxworthy, 1979]. The flow velocity includes the background current velocity and the tidal current velocity. Hence, the second term changing its magnitude and direction several times per day, can change the flow mode and affect the generation of SIWs. In the KGS, the flow velocity averages 0.06–0.26 m/s and reaches 0.5 m/s at the peak [Morozov *et al.*, 2003]. At the same time, the velocities of tidal currents vary in the range up to 0.5 m/s, which can potentially create a total magnitude of the flow velocity vector up to 1 m/s.

The active use of methods of satellite oceanography, in particular measurements of spaceborne SARs, the quantity and quality of information about the areas of formation and spatial characteristics of SIWs has significantly increased [Dubina and Mitnik, 2007; Jackson, 2004; Kozlov *et al.*, 2015a; Kozlov and Kuzmin, 2022; Lavrova *et al.*, 2009, 2011]. A large volume of satellite data allows to use statistical methods to determine the areas of regular formation of SIWs and to study their distribution and evolution.

This paper presents the analysis results of the SIW properties in the KGS obtained based on the processing of Sentinel-1 SAR data in August–September 2021. The obtained results are compared with the detailed bottom topography of the area and the characteristics of tidal currents from the Arc5km2018 model [Erofeeva and Egbert, 2020].

2. Data and methods

To analyze the characteristics of the SIW field in the KGS, Sentinel-1 A/B SAR data were used in the IW (Interferometric Wide Swath) and EW (ExtraWide) modes with a spatial resolution of 20 m and 40 m, respectively. SAR images were obtained from the archives of the Copernicus Marine Open Access Hub (<https://scihub.copernicus.eu>). A total of 47 SAR images were processed, 11 of which possessed clear surface manifestations of SIWs. Table 1 presents summary data on the number of processed images in August–September 2021. Earlier studies of this region have shown that the largest number of SIW trains is observed in September [Kozlov *et al.*, 2015a], so special attention was paid to the analysis of the data in late summer – early autumn.

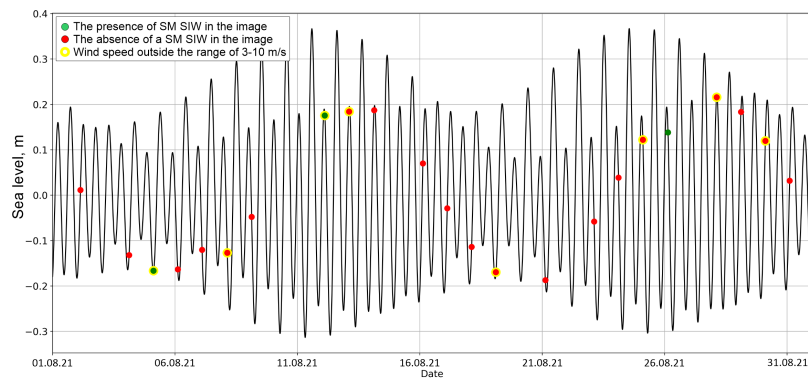
Table 1. Main characteristics of satellite radar observations in the Kara Gates Strait.

Month, 2021	Count of RI	Count of packet of SIW
August	23	10
September	24	34

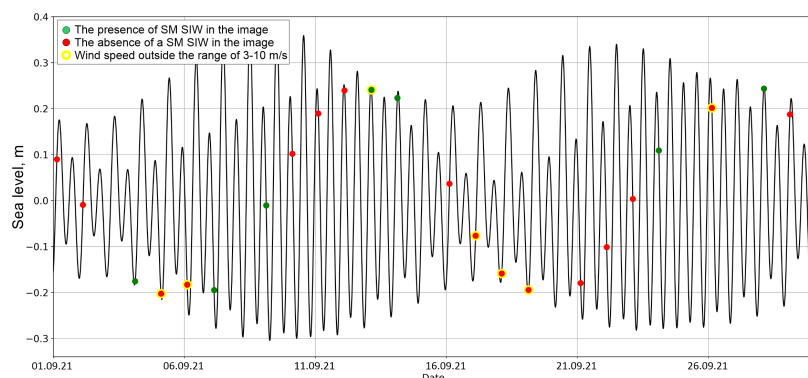
Satellite radar monitoring of the sea surface can be complicated at strong winds. According to the modeling results in the Kara Gates Strait, the maximum wave height can reach 6–7 m at a wind speed of 15 m/s [Myslenkov *et al.*, 2021a,b]. At such wind speeds, SMs of SIWs become indistinguishable in SAR images. The optimal range of wind speeds for observing the SMs of SIWs is 3–10 m/s. A data set of ASCAT METOP-A/B/C satellite scatterometer was used to assess the background wind conditions. The time interval

between the ASCAT and Sentinel-1 flights ranged from 1.5 to 8 hours. In total, the wind speed went beyond the optimal range for 15 days during the research period (Figure 1), while for two days wind conditions were stormy (wind speed >25 m/s).

To analyze the background tidal conditions, data from the Arc5km2018 model with a horizontal resolution of 5 km were used. The strait has relatively small horizontal dimensions (no more than 50 km), and the maximum difference in the tidal phase across the strait is 22 minutes. Hence, the analysis of the model data was carried out only for the central point of the strait (70.4688°N, 57.9513°E). The exception was the spatial distribution of the tidal ellipses for the lunar semidiurnal tide M_2 .



(a)



(b)

Figure 1. Tidal fluctuations of sea level [m] in a) August and b) September 2021 according to the Arc5km2018 model with points marking the time of satellite observations. Green (red) markers show the time when SIW signatures were present (absent) in satellite images

The coverage of the strait by satellite data in August 2021 was very uneven in time, most of the images were obtained in the second half of the month (Figure 1a). In September 2021, the coverage was more uniform (Figure 1b) and, on average, there was one SAR snapshot every second day. The acquisition time of satellite data was nearly the same, around 03:00 UTC. Since an M_2 tidal period (12.4 hours) slightly exceeds half a day, satellite imagery enabled to observe the characteristics of the SIWs at different phases of spring-neap cycle (Figure 1).

To assess the impact of bottom topography inhomogeneities on SIW propagation, ocean bathymetry data digitized from the 1:500000 scale navigation map of the DNao MD RF were used. This map was published in 1995 with the last correction in 2016. The distance between adjacent marks on the navigation map is about 5 km. For further analysis, digitized data were transformed into a regular grid with a step of 1' using linear interpolation. Bathymetry map (Figure 2a) and the dimensionless slope of the bottom relief (Figure 2b) are constructed on the basis of the resulting array. The dimensionless slope of

the bottom relief was calculated as the ratio of the depth difference to the distance between adjacent grid nodes.

3. Analysis of background conditions

The Kara Gates Strait has a complex heterogeneous bottom (Figure 2a). The area can be divided into deep-water (>100 m) and shallow-water (<100 m) parts. The first is a broken depression, which, twisting, passes through the strait. According to [Morozov *et al.*, 2017] and [Kopyshov *et al.*, 2021], a large number of small-scale topographic inhomogeneities are observed in the strait. These features are often smoothed out by standard bottom topography data sets, such as IBCAO [Jakobsson *et al.*, 2012], etc. Analyzing the dimensionless slope data (Figure 2b), its elevated values are found in the southeastern part of the strait and in its central part. Also, strong heterogeneities are observed at the exit of the strait from the Kara Sea, as well as at the entrance of the strait from the Barents Sea, as well as in its central part. There is also a pronounced slope off the east coast of Vaygach Island, however, this region was not considered in our work.

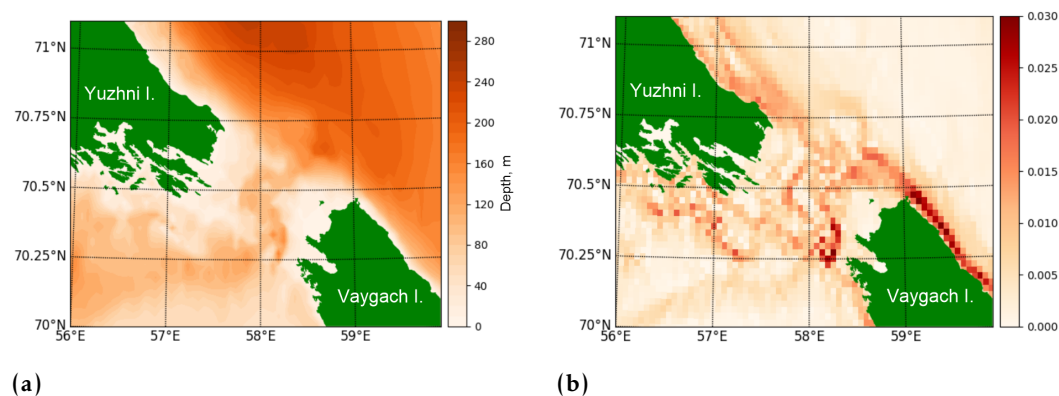


Figure 2. Bottom topography of the Kara Gates Strait: a) total depths and b) dimensionless slope

To study the objects of the internal tide evolution, it is important to know its characteristics. As already mentioned before, the tidal harmonic M_2 prevails in the study area [Kagan and Timofeev, 2015; Morozov *et al.*, 2008, 2017]. Figure 3 shows M_2 tidal ellipses from the Arc5km2018 model.

The tidal ellipses in the strait differ very much from each other both in magnitude and in their geometry. In the eastern part of the strait, large values of the maximum tidal flow velocity of 0.4 m/s are observed. In the southeastern part of the strait, they are very elongated and play a key role during the peak moments of the tidal cycle. In the northeastern part, on the contrary, the ellipses have a more rounded shape meaning the tidal flow is more uniform in time in this subregion.

In the central part of the strait, especially at the entrance and exit from it, tidal ellipses have very small sizes (magnitude < 0.01 m/s), which indicates their reduced influence on the overall picture of currents. In the southwestern part of the district, near the southern part of Novaya Zemlya, tidal ellipses also have an elongated shape and reach 0.15 m/s at the peak of the tidal flow velocity.

It is worth paying attention to the fact that due to the different geometry and orientation of tidal ellipses, the maximum values of tidal velocities are not achieved synchronously. It means that the tidal conditions favorable for the SIW generation occur at different times in different parts of the strait. Moreover, the maximum value of the tidal velocity can vary greatly during spring-neap cycle. In such case, the maximum deviation of the instant flow velocity from its average value will also vary significantly, which in turn would affect the transition of the flow to supercritical mode.

The superposition of the intense tidal dynamics and the complex bottom relief with a large number of underwater elevations near the critical latitude should naturally lead to the formation of multidirectional packets of SIWs [Li *et al.*, 2019; Morozov *et al.*, 2017],

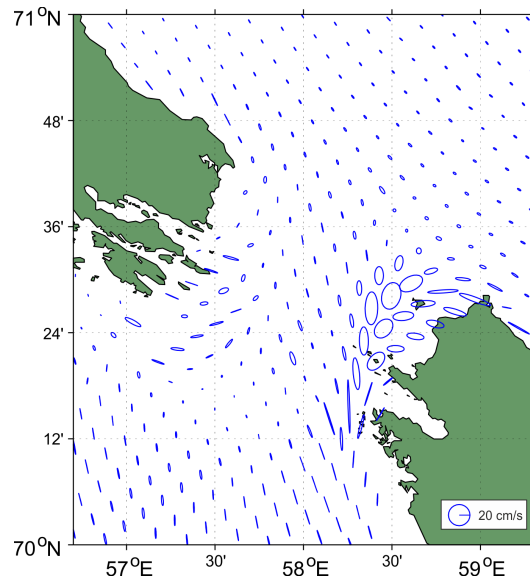


Figure 3. M_2 tidal ellipses obtained from the Arc5km2018 model for August 2021.

as confirmed both by full-scale *in situ* measurements [Morozov *et al.*, 2017] and satellite observations [Kozlov *et al.*, 2015a].

3.1. Results of satellite observations

In total, during the analysis of 47 SAR images, 10 SIW packets were identified in August 2021 and 37 – in September 2021. Such ratios of the number of recorded SIW manifestations by month were also observed in earlier studies [Kozlov *et al.*, 2015a,b].

An overall map showing leading waves of all identified SIWs in the KGS is shown in Figure 4. About 40% of all observed SIWs were recorded over the deep-water part of the strait, which makes up ~23% of the total area of the strait. The geographic areas where SIW trains were observed over the shallow part of the strait can be divided into three regions (Figure 4).

In region 1, 7 manifestations of SIWs were registered on ~120 km². Most packets of SIWs are directed across the strait and across isobaths to the northwest, which is a very interesting feature rarely described in the literature. The only wave train directed to the southwest is characterized by a much longer leading wave. It is located approximately in the center of an elongated shoal/hill with depths of about 30–40 m, oriented across the strait and surrounded by deep-water areas on three sides.

The smallest number of SIW trains was detected in the region 2 (5 packets per ~400 km²), where large amplitudes of the tidal current are observed (up to 0.5 m/s), while the bottom is fairly uniform (dimensionless slope is less than 0.001). The SIWs registered in this area were directed to the south, east and west, thus spreading primarily across the strait, while having very short lengths of the leading wave ~ 1 km. Some of the waves, in the northwestern part of the area, were most likely generated either over a sloping bottom or over the deeper parts of the strait. These waves have a much longer length of the leading wave than those found to the east.

The largest number of SIWs was registered in the region 3. Here, 12 manifestations of SIWs per ~100 km² were registered. The directions of wave propagation in this region were more diverse compared to other areas. Yet, most waves were predominantly directed to the southwest. The values of the dimensionless slope here are rather average, around 0.015. An interesting feature is the fact that in the northwestern sector of this region the waves are directed across the strait towards Vaygach Island, while in the central sector – along the strait, towards the Barents Sea.

The main difference between the regions 1, 3 and the region 2 is the availability of steeper area where slope values exceed 0.015. The amplitudes of tidal currents in regions 1

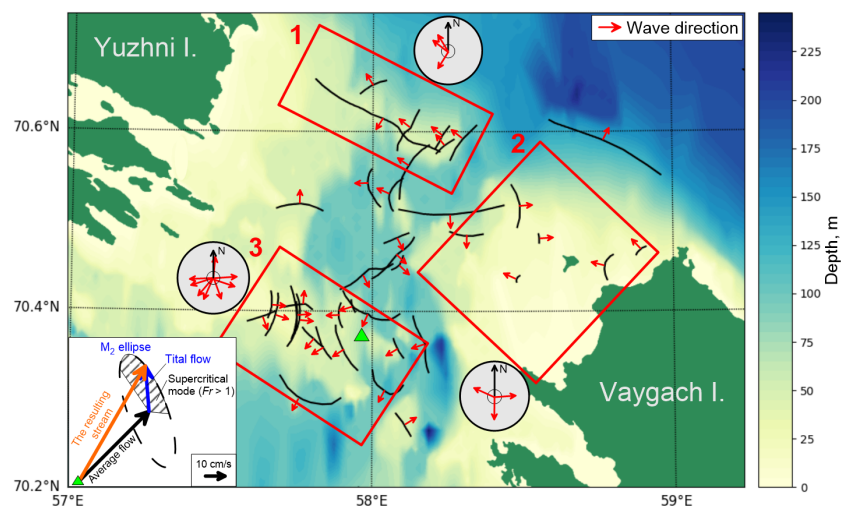


Figure 4. The position of the surface manifestations of the leading waves in the packets of SIWs in August-September 2021. The main shallow water regions where the SIW registration took place are highlighted with red frames and numbered. Each region has a diagram of SIW propagation direction shown by red arrows in grey circles. The graph in the lower left corner schematically shows the formation of resulting supercritical flow ($c_0 = 0.5$ m/s, the average flow velocity of 0.3 m/s, the magnitude of the tidal current fluctuations of 0.3 m/s) in the place marked by a green triangle.

and 3 are slightly lower than 0.15–0.20 m/s, however, due to the heterogeneous topography, the conditions for the destruction of the IT are favorable. Moreover, the region 3 is also characterized by a large number of secluded seamounts [Kopyshov et al., 2021; Morozov et al., 2017], explaining the variety of SIW propagation directions in this region.

As already mentioned above, generation of SIWs should occur near the critical flow regime ($Fr \sim 1$). In the strait, the total current velocity consists of the mean flow from the Barents Sea to the Kara Sea, and the tidal current. The latter term is variable in time, which leads to a change in the resulting flow velocity vector from subcritical to supercritical Fr values, and vice versa. This process is illustrated by the vector diagram in the lower left corner shown in Figure 4. It is constructed for a single point in the strait marked with a green triangle. The schematic shown in Figure 4 was produced by assuming the mean flow of 0.3 m/s, the amplitude of the tidal current velocity of 0.3 m/s, and the phase speed of linear internal wave of 0.5 m/s obtained for the background stratification conditions in the strait.

Let us now consider some features of the spatial characteristics of the SIWs. Figure 5 shows histogram distribution of the length of the leading front (Figure 5a) and the SIW packet width (Figure 5b) characterizing the horizontal dimensions of these structures. The most common were SIW packets with a leading front length of about 5 km. The maximum values of this property reached 26 km and were observed in the region 1 at the exit of the strait. For packet widths, the peak value is 2 km while the maximum width of the SIW packets is 6.5 km. The widest structures were recorded over the deep-water regions and in the northern part of region 3.

The spatial differences noted above directly depend on the characteristics of the slope, since the generation of packets with a longer length of the leading front should occur on longer slopes, which are observed at the exit of the strait from the Kara Sea side. The width of the packet is determined by the number of waves in the packet and their wavelength. The first is determined by the lifetime of the wave packet, while the second largely depends on the horizontal size of the obstacle [Kozlov and Kuzmin, 2022]. The horizontal lengths of obstacles in the strait are very different from each other and, usually, they have a relatively small scale of 0.1–1 km. The available bathymetric data are not enough detailed to perform

a more complete analysis of the relationship of the spatial properties of the observed SIW trains with the geometric characteristics of the bottom topography.

Lastly, it is also important to accent here that satellite imagery covers different phases of the spring-neap tidal cycle, allowing to observe 5–7 different episodes of this cycle (Figure 1). Surface manifestations of SIWs were recorded equally often both during the spring and the neap tides. As obtained, the registration of many SIW packets occurred a few hours after the onset of low/high water.

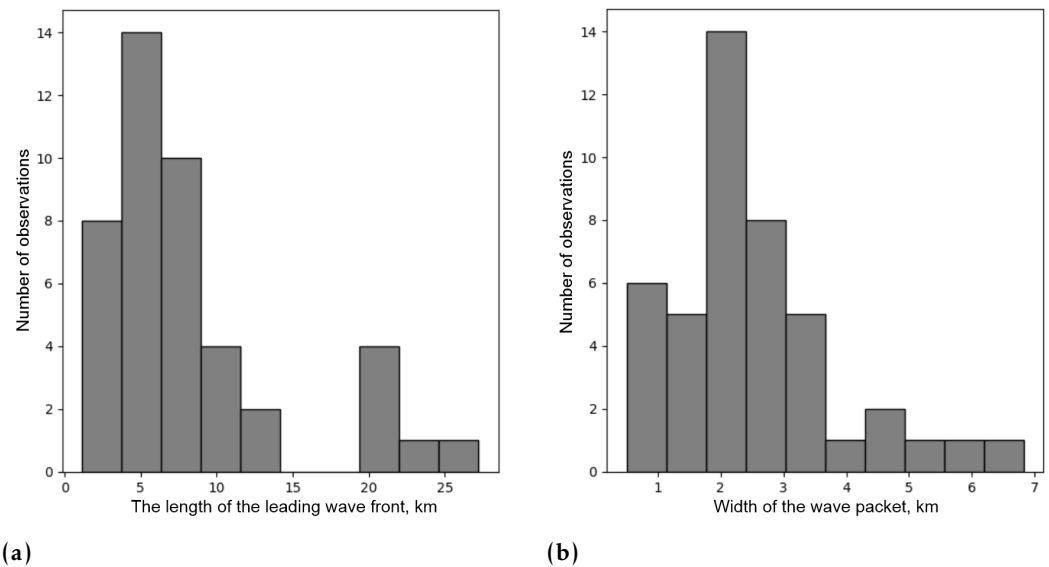


Figure 5. Histograms a) the length of the front of the leading waves in packets of SIW, and b) their width.

4. Discussion

In this paper, the peculiarities of SIW generation and propagations in the Kara Gates Strait were considered. As shown, most of the SIW trains were registered at the entrance to the strait in regions 1 and 3, as well as in the central deep-water part. Most often the packets of SIWs were found near pronounced inhomogeneities of the bottom topography where amplitudes of tidal velocity exhibited relatively high values. In such areas, SIWs could be generated either via the lee wave mechanism when the total current flow exceeds critical value ($Fr > 1$), or in the transcritical regime when the Froude number passes over a critical value [da Silva, J. C. B. and Helfrich, 2008]. In any case, we presume that modulation of the resulting current flow by the changing tidal current velocity is the key factor governing the generation of NIWs in the study region.

An interesting fact is that with a certain ratio of the intensity of the mean flow, the tidal flow, the IW phase velocity, as well as the orientation of the tidal ellipse, the “permitted zone”, where the supercritical flow regime is observed (Figure 4, the dashed fill in the diagram of the resulting flow formation) may appear in the opposite direction. This means that the generation of SIW packets will occur not once per semidiurnal tidal period, but at least twice – at high and low tide. Also, the M_2 tidal harmonic is dominant, but not the only one in the study area. When additional ellipses of other harmonics are superimposed, the resulting tidal velocity can change in a rather complicated way within both a semidiurnal period and a spring-neap cycle. This may lead to an increase in the number of “permitted zones” of SIW generation, as well as their overlap with each other at nearby locations.

Also, the question of the particular tidal phase at which SIWs are generated remains poorly understood. It is known from theory that this begins at the moment of the onset of the supercritical flow ($Fr \sim 1$) and occurs until the value of the flow velocity decreases to the subcritical regime [Jackson et al., 2012; Maxworthy, 1979]. It is assumed that at this moment there is an intensive pumping of energy, while the flow of the jet onto the

topographic inhomogeneity causes the shape of the isopycnic surfaces to change. The further the stream is in the supercritical state, the more intense the SIWs packet should be. If the passage of the "permitted zone" occurs very quickly, for example, when the tidal ellipses are very elongated, the generated internal waves should be less intense, but experimental confirmation of the latter fact is not known to us.

The Kara Gates Strait is also interesting because it has a strong frontal zone. It separates the flow of the relatively warm Barents Sea water, which usually occupies the central part of the strait, and the cold counter-current from the Kara Sea, which spreads along the southern coast of Novaya Zemlya to the southwest. Their interaction is complex, which generates a quasi-stable vertical inhomogeneity of velocities [McClimans *et al.*, 2000; Morozov *et al.*, 2017]. However, we do not consider SIW generation in the KGS owing to existence of the frontal zone in this work.

5. Conclusions

The paper presents the results of spaceborne SAR data processing to investigate properties of short-period internal waves in the Kara Gates Strait. Analysis of 47 Sentinel-1A/B SAR images for August-September 2021 allowed to identify 44 surface manifestations of SIWs. It was shown that a large number of SIW packets was observed near sloping bottom with relatively high values of dimensionless slope and moderate amplitudes of tidal current velocities in the shallow areas of the strait.

Manifestations of SIW were recorded in large numbers both over the deep-water parts of the strait (>100 m) and over its shallow areas (from 30 to 100 m). Analysis of satellite data showed that SIW was actively registered both during spring (about half of all packets) and neap tides. As suggested, spring-neap variability of tidal current intensity mainly affects the intensity of the initial pycnocline disturbance from which SIW are generated later. As such, the locations of SIW generation could be more or less constant within a spring-neap cycle, but the horizontal and vertical properties of SIW should be enhanced during spring tide. Nevertheless, spatial properties of SIWs such as their wavelength and the length of the leading front should also depend on the horizontal dimensions of the obstacles.

Analysis of the satellite data in conjunction with tidal model predictions of sea level fluctuations showed that SIW packets in the strait are recorded equally frequent at different phases of the semidiurnal tide.

Acknowledgements

The study was carried out within the framework of the state task No. FNNN-2021-0010. Sentinel-1A/B satellite data were obtained from the Copernicus Marine Open Access Hub (<https://scihub.copernicus.eu>). Wind speed data of ASCAT METOP-A/B/C scatterometers were obtained from the National Environmental Satellite, Data, and Information Service (NESDIS) Satellite Application and Research Center from (<https://manati.star.nesdis.noaa.gov>).

The part of the study related to the calculation of tidal conditions was funded by the state task FMWE-2021-0015.

References

- Boegman, L., and M. Stastna (2019), Sediment Resuspension and Transport by Internal Solitary Waves, *Annual Review of Fluid Mechanics*, 51(1), 129–154, <https://doi.org/10.1146/annurev-fluid-122316-045049>.
- Carr, M., P. Sutherland, A. Haase, K.-U. Evers, I. Fer, A. Jensen, H. Kalisch, J. Berntsen, E. Părău, Ø. Thiem, and P. A. Davies (2019), Laboratory Experiments on Internal Solitary Waves in Ice-Covered Waters, *Geophysical Research Letters*, 46(21), 12,230–12,238, <https://doi.org/10.1029/2019GL084710>.
- Czipott, P. V., M. D. Levine, C. A. Paulson, D. Menemenlis, D. M. Farmer, and R. G. Williams (1991), Ice Flexure Forced by Internal Wave Packets in the Arctic Ocean, *Science*, 254(5033), 832–835, <https://doi.org/10.1126/science.254.5033.832>.

- da Silva, J. C. B., and K. R. Helfrich (2008), Synthetic Aperture Radar observations of resonantly generated internal solitary waves at Race Point Channel (Cape Cod), *Journal of Geophysical Research: Oceans*, 113(C11), <https://doi.org/10.1029/2008JC005004>.
- D'Asaro, E. A. (2022), How do Internal Waves Create Turbulence and Mixing in the Ocean?, *ESS Open Archive*, <https://doi.org/10.1002/essoar.10511843.1>, (Preprint).
- Dubina, V. A., and L. M. Mitnik (2007), Internal waves in the Sea of Japan: spatial-temporal distribution and characteristics according to satellite remote sensing data, *Issledovanie Zemli iz Kosmosa*, 3, 37–46 (in Russian).
- Edge, W. C., N. L. Jones, M. D. Rayson, and G. N. Ivey (2021), Calibrated Suspended Sediment Observations Beneath Large Amplitude Non-Linear Internal Waves, *Journal of Geophysical Research: Oceans*, 126(12), <https://doi.org/10.1029/2021jc017538>.
- Erofeeva, S., and G. Egbert (2020), Arc5km2018: Arctic Ocean Inverse Tide Model on a 5 kilometer grid, 2018, <https://doi.org/10.18739/A21R6N14K>.
- Fer, I., Z. Koenig, I. E. Kozlov, M. Ostrowski, T. P. Rippeth, L. Padman, A. Bosse, and E. Kolås (2020), Tidally Forced Lee Waves Drive Turbulent Mixing Along the Arctic Ocean Margins, *Geophysical Research Letters*, 47(16), <https://doi.org/10.1029/2020gl088083>.
- Garwood, J., R. Musgrave, and A. Lucas (2020), Life in Internal Waves, *Oceanography*, 33(3), 38–49, <https://doi.org/10.5670/oceanog.2020.313>.
- Jackson, C., J. da Silva, and G. Jeans (2012), The Generation of Nonlinear Internal Waves, *Oceanography*, 25(2), 108–123, <https://doi.org/10.5670/oceanog.2012.46>.
- Jackson, C. R. (2004), *An atlas of internal solitary-like waves and their properties*, 2nd ed., Global Ocean Associates, Alexandria.
- Jakobsson, M., L. Mayer, B. Coakley, J. A. Dowdeswell, S. Forbes, B. Fridman, H. Hodnesdal, R. Noormets, R. Pedersen, M. Rebecco, H. W. Schenke, Y. Zarayskaya, D. Accettella, A. Armstrong, R. M. Anderson, P. Bienhoff, A. Camerlenghi, I. Church, M. Edwards, J. V. Gardner, J. K. Hall, B. Hell, O. Hestvik, Y. Kristoffersen, C. Marcussen, R. Mohammad, D. Mosher, S. V. Nghiem, M. T. Pedrosa, P. G. Travaglini, and P. Weatherall (2012), The International Bathymetric Chart of the Arctic Ocean (IBCAO) Version 3.0, *Geophysical Research Letters*, 39(12), <https://doi.org/10.1029/2012GL052219>.
- Kagan, B. A., and A. A. Timofeev (2015), Spatial variability in the drag coefficient and its role in tidal dynamics and energetics, a case study: The surface M₂ tide in the subsystem of the Barents and Kara Seas, *Izvestiya, Atmospheric and Oceanic Physics*, 51(1), 98–111, <https://doi.org/10.1134/s0001433814060103>.
- Kagan, B. A., E. V. Sofina, and A. A. Timofeev (2018), Critical Latitude in Tidal Dynamics Using the Kara Sea as an Example, *Izvestiya, Atmospheric and Oceanic Physics*, 54(2), 206–212, <https://doi.org/10.1134/s000143381802010x>.
- Konyaev, K. V. (2000), Internal tide at the critical latitude, *Izvestiya. Atmospheric and Oceanic Physics*, 36(3), 363–375 (in Russian).
- Kopyshov, I. O., I. E. Kozlov, V. R. Zhuk, A. V. Artamonova, K. P. Silvestrova, O. S. Mekhova, A. I. Korzhenovskaya, D. I. Frey, A. G. Jamalova, P. V. Gaisky, A. A. Osadchiev, and N. B. Stepanova (2021), Study of high-amplitude internal waves in The Kara Gate Strait in August 2021, in *X International conference «Marine Research and Education» MARESEDU-2021*, vol. 1, pp. 238–241, PoliPRESS, Tver (in Russian).
- Kozlov, I., V. Kudryavtsev, E. Zubkova, O. Atadzhanova, A. Zimin, D. Romanenkov, A. Myasoedov, and B. Chapron (2015a), SAR observations of internal waves in the Russian Arctic seas, in *2015 IEEE International Geoscience and Remote Sensing Symposium (IGARSS)*, IEEE, <https://doi.org/10.1109/IGARSS.2015.7325923>.
- Kozlov, I. E., and A. V. Kuzmin (2022), New regions of short-period internal wave generation in the Laptev Sea revealed from Sentinel-1 data, *Sovremennye problemy distantsionnogo zondirovaniya Zemli iz kosmosa*, 19(4), 280–290, <https://doi.org/10.21046/2070-7401-2022-19-4-280-290>.

- Kozlov, I. E., V. N. Kudryavtsev, E. V. Zubkova, A. V. Zimin, and B. Chapron (2015b), Characteristics of short-period internal waves in the Kara Sea inferred from satellite SAR data, *Izvestiya, Atmospheric and Oceanic Physics*, 51(9), 1073–1087, <https://doi.org/10.1134/s0001433815090121>.
- Kudryavtsev, V., I. Kozlov, B. Chapron, and J. A. Johannessen (2014), Quad-polarization SAR features of ocean currents, *Journal of Geophysical Research: Oceans*, 119(9), 6046–6065, <https://doi.org/10.1002/2014jc010173>.
- Lavrova, O. Y., M. I. Mityagina, and K. D. Sabinin (2009), Manifestation of internal waves on the sea surface in the northeastern part of the Black Sea, *Issledovanie Zemli iz Kosmosa*, (6), 49–55 (in Russian).
- Lavrova, O. Y., M. I. Mityagina, and K. D. Sabinin (2011), Study of internal wave generation and propagation features in non-tidal seas based on satellite synthetic aperture radar data, *Doklady Earth Sciences*, 436(3), 165–169 (in Russian).
- Li, Q., H. Wu, H. Yang, and Z. Zhang (2019), A numerical simulation of the generation and evolution of nonlinear internal waves across the Kara Strait, *Acta Oceanologica Sinica*, 38(5), 1–9, <https://doi.org/10.1007/s13131-019-1437-z>.
- Maxworthy, T. (1979), A note on the internal solitary waves produced by tidal flow over a three-dimensional ridge, *Journal of Geophysical Research: Oceans*, 84(C1), 338–346, <https://doi.org/10.1029/jc084ic01p00338>.
- McClimans, T. A., D. R. Johnson, M. Krosshavn, S. E. King, J. Carroll, and Ø. Grenness (2000), Transport processes in the Kara Sea, *Journal of Geophysical Research: Oceans*, 105(C6), 14,121–14,139, <https://doi.org/10.1029/1999jc000012>.
- Morozov, E., and D. Frey (2023), Strait of Kara Gates: A Region of Strong Internal Tides in the Arctic Seas, *Russian Journal of Earth Sciences*, 23(3), 1–7, <https://doi.org/10.2205/2023es000860>.
- Morozov, E. G., and V. T. Paka (2010), Internal waves in a high-latitude region, *Oceanology*, 50(5), 668–674, <https://doi.org/10.1134/s0001437010050048>.
- Morozov, E. G., and S. V. Pisarev (2002), Internal tides at the Arctic latitudes (numerical experiments), *Oceanology*, 42(2), 165–173.
- Morozov, E. G., and S. V. Pisarev (2004), Internal waves and polynya formation in the Laptev Sea, *Doklady Earth Sciences*, 397(3), 1–4 (in Russian).
- Morozov, E. G., S. V. Pisarev, and S. Y. Erofeeva (2002), Internal tidal waves in the Arctic seas of Russia, in *Surface and internal waves in Arctic seas. Part II. Internal waves in the Arctic seas of Russia*, pp. 214–234, Gidrometeoizdat, Saint Petersburg (in Russian).
- Morozov, E. G., V. G. Neiman, and A. D. Shcherbinin (2003), Internal tide in the Kara Strait, *Doklady Earth Sciences*, 393(9), 1312–1314.
- Morozov, E. G., V. T. Paka, and V. V. Bakhanov (2008), Strong internal tides in the Kara Gates Strait, *Geophysical Research Letters*, 35(16), <https://doi.org/10.1029/2008GL033804>.
- Morozov, E. G., I. E. Kozlov, S. A. Shchuka, and D. I. Frey (2017), Internal tide in the Kara Gates Strait, *Oceanology*, 57(1), 8–18, <https://doi.org/10.1134/s0001437017010106>.
- Moum, J. N., D. M. Farmer, W. D. Smyth, L. Armi, and S. Vagle (2003), Structure and Generation of Turbulence at Interfaces Strained by Internal Solitary Waves Propagating Shoreward over the Continental Shelf, *Journal of Physical Oceanography*, 33(10), 2093–2112, [https://doi.org/10.1175/1520-0485\(2003\)033<2093:sagota>2.0.co;2](https://doi.org/10.1175/1520-0485(2003)033<2093:sagota>2.0.co;2).
- Moum, J. N., J. M. Klymak, J. D. Nash, A. Perlin, and W. D. Smyth (2007), Energy Transport by Nonlinear Internal Waves, *Journal of Physical Oceanography*, 37(7), 1968–1988, <https://doi.org/10.1175/jpo3094.1>.
- Myslenkov, S., V. Platonov, A. Kislov, K. Silvestrova, and I. Medvedev (2021a), Thirty-Nine-Year Wave Hindcast, Storm Activity, and Probability Analysis of Storm Waves in the Kara Sea, Russia, *Water*, 13(5), 648, <https://doi.org/10.3390/w13050648>.
- Myslenkov, S. A., V. S. Platonov, K. P. Silvestrova, and S. A. Dobrolyubov (2021b), Increase in Storm Activity in the Kara Sea from 1979 to 2019: Numerical Simulation Data, *Doklady Earth Sciences*, 498(2), 502–508, <https://doi.org/10.1134/s1028334x2106012x>.

- Phillips, O. M. (1980), *The Dynamics of the Upper Ocean (Cambridge Monographs on Mechanics)*, 344 pp., Cambridge University Press.
- Pineda, J. (1991), Predictable Upwelling and the Shoreward Transport of Planktonic Larvae by Internal Tidal Bores, *Science*, 253(5019), 548–549, <https://doi.org/10.1126/science.253.5019.548>.
- Sabinin, K. D., A. N. Serebryanyi, and A. A. Nazarov (2004), Intensive internal waves in the World Ocean, *Oceanology*, 44(6), 753–758 (in Russian).